MOLECULAR AND CELLULAR BIOLOGY, Apr. 2005, p. 2995–3006 Vol. 25, No. 8
0270-7306/05/$08.00+0 doi:10.1128/MCB.25.8.2995–3006.2005

Scaffold Attachment Factor B1 Functions in Development, Growth, and Reproduction

Margarita Ivanova,† Klaudia M. Dobrzycka, Shiming Jiang, Kai Michaelis,‡ Rene Meyer, Kaiyan Kang, Brian Adkins,§ Oleg A. Barski,† Simeen Zubairy, Jana Divisova, Adrian V. Lee, and Steffi Oesterreich*

Departments of Medicine and Molecular and Cellular Biology, Breast Center, Baylor College of Medicine, and Methodist Hospital, Houston, Texas

Received 22 September 2004/Returned for modification 20 November 2004/Accepted 30 December 2004

Scaffold attachment factor B1 (SAFB1) is a multifunctional protein that can bind both DNA and RNA and is involved in RNA processing and stress response. In addition, SAFB1 contains a transcriptional repression domain and can bind certain hormone receptors and repress their activity. To assess the role of SAFB1 in vivo, we generated SAFB1 mutant mice through targeted deletion in embryonic stem cells. While viable homozygous mutant (SAFB1$^{-/-}$) mice were obtained, genotypic distribution indicated that homozygous deficiency resulted in both prenatal and neonatal lethality. Mice lacking SAFB1 exhibited dwarfism, as a result of in utero growth retardation, and had low serum insulin-like growth factor 1 (IGF1) levels. In agreement with the previous characterization of SAFB1 as a corepressor for hormone receptors, we found that SAFB1$^{-/-}$ mice displayed dramatic defects in the development and function of the reproductive system. Male SAFB1 null mice were infertile, apparently because of low circulating levels of testosterone. SAFB1$^{-/-}$ testes were small and showed progressive degeneration of the germinal epithelium, increased apoptosis of germ cells, and Leydig cell hyperplasia. SAFB$^{-/-}$ female mice were subfertile and showed progressive infertility, in part because of defects in oviductal transport and reduced numbers of follicles. Immortalized SAFB1$^{-/-}$ mouse embryonic fibroblasts showed cell-intrinsic defects including increased transcriptional estrogen receptor α activity and enhanced responsiveness to IGF1. Together, these in vivo findings establish a critical role for SAFB1 in development, growth regulation, and reproduction.

Scaffold attachment factor B1 (SAFB1) was originally cloned by Renz and Fackelmayer (42) on the basis of its ability to bind to AT-rich scaffold-matrix attachment regions (S/MARs). We subsequently cloned SAFB1 on the basis of its ability to bind and repress the small heat shock protein 27 promoter (38). We also recently cloned a related family member termed SAFB2 (46). SAFB1 is 74% homologous to SAFB2, and the major functional domains are highly conserved. The human genes for SAFB1 and SAFB2 are adjacent to each other on chromosome 19p13.3 and are arranged in a bidirectional divergent configuration. The transcriptional start sites of the two paralogues are separated by a short (<500-bp) GC-rich intergenic region that has been shown to function as a bidirectional promoter (46).

SAFBs are multifunctional proteins that contain numerous highly conserved functional domains (37). SAFB1 has an RNA recognition motif (RRM) (47) and can also interact with a number of RNA processing proteins (13, 51). Since SAFB1 also interacts with RNA polymerase II, it has been suggested that it may be part of a "transcriptosome" complex, bringing together transcription and RNA processing (36). SAFB1 has a nuclear localization signal (NLS), and we (38) and others (42) have shown that it is a nuclear protein that copurifies with chromatin and nuclear matrix protein fractions.

Both SAFB1 and SAFB2 contain an N-terminal SAF-Box, which is a homeodomain-like DNA-binding motif that interacts with S/MARs (3, 25). S/MARs have been proposed to potentially contribute to higher-order chromatin structure by mediating the attachment of chromatin to the nuclear matrix, thereby folding chromatin into topologically independent loop domains (5); however, more work is needed to clearly define the role of S/MARs in chromatin remodeling and transcriptional regulation. While the exact roles of S/MAR-binding proteins in transcription and recombination have yet to be defined, models are being generated that will facilitate their analysis. For example, SATB1, a thymocyte-specific S/MAR-binding protein, has recently been deleted in embryonic stem (ES) cells (2). SATB1-null mice die at 3 weeks of age and display multiple defects at almost every developmental stage of T-cell development. DNA microarray analysis confirmed that SATB1 is essential for the spatially and temporally correct transcription of multiple genes in thymocytes and peripheral T cells (2). Further study of models like this should reveal the role of S/MAR-binding proteins in development.

SAFB proteins are also estrogen receptor α (ERα) corepressors. Corepressors and coactivators, collectively called cofactors, are defined as proteins that interact with a nuclear receptor and inhibit or activate its transcriptional activity (14). There is an increasing literature showing that not only ERα (12, 15) but also its cofactors are critically involved in sexual

* Corresponding author. Mailing address: Baylor College of Medicine, Breast Center, One Baylor Plaza, Houston, TX 77030. Phone: (713) 798-1623. Fax: (713) 798-1642. E-mail: steffio@breastcenter.tmc.edu.

† Present address: University of Louisville, Louisville, Ky.

‡ Present address: Institute for Molecular Biology of Infections, D-97070 Würzburg, Germany.

§ Present address: Howard University, Washington, D.C.

maturation and reproduction. For example, deletion of the ERα coactivators SRC2 (21) and SRC3 (30) resulted in subfertility in female mice, whereas deletion of the corepressor RIP140 led to complete infertility because of failure of the mature follicle to be released upon ovulation (52). Mouse models of cofactor deficiency often display pleiotropic phenotypes, most likely because of their ubiquitous expression and the promiscuous nature of their coactivation or corepression of nuclear receptors.

To better understand the physiological role of SAFB1, we generated SAFB1$^{-/-}$ mice by targeted gene deletion. Our studies show that SAFB1 plays an important role during embryonic development and in the formation and function of the reproductive system. SAFB1$^{-/-}$ mice show in utero growth retardation, which is associated with low insulin-like growth factor 1 (IGF1) levels. Pleiotropic defects, caused by altered hormone levels and cell-autonomous defects, result in subfertility and infertility in females and males, respectively. Collectively, these phenotypes clearly establish a role for SAFB1 in embryonic development, as well as in the regulation of reproduction.

MATERIALS AND METHODS

Gene targeting and generation of SAFB1 knockout mice. Murine genomic SAFB1 DNA was derived from a 129/Sv phage genomic library (kindly provided by F. DeMayo, Baylor College of Medicine [BCM]), subcloned, and sequenced. Homology with the GenBank entry with accession number XM_128715 (*Mus musculus* hypothetical protein E130307D12; Sanger Center ENSMUSG00000042128) was confirmed. The murine clone was sent to Genome Systems Inc. (St. Louis, Mo.), where fluorescence in situ hybridization analysis was performed.

To generate the targeting vector, a 5′ homology arm of 5 kb was amplified from the murine SAFB1 clone with primers 5′-GGCGAGCTCATGGACATC AGTGTGCTGGATGAGG-3′ and 5′-GGCGTCGACTCACCTAGTTATGTC TGGCCCCACGCTACTCGTGG-3′ and cloned into the SacI/SalI sites of the targeting vector pNTRLacZPGKneolox. A 4-kb 3′ arm was amplified with primers 5′-GGCGCGGCCGCTAACTAGGTGACTGTGGTGATGGACAAGTCC AAAG-3′ (with STOP codons in all three reading frames) and 5′-GGCCCGC GGATGCTGTCCTTCTCTGTCTCCCAT-3′ and cloned into NotI/SacII sites. The internal ribosome entry site (IRES)-*lacZ* (β-galactosidase)-*neo*-selectable cassette was placed between these two homology arms. Successful recombination resulted in deletion of exons 7 through 22 starting at amino acid (aa) 297.

The linearized targeting construct was electroporated into 129/Sv ES cells, and 329 G418-resistant clones were screened for homologous recombination by Southern blot analysis. A 700-bp probe that was outside of the original targeting construct was derived from the murine genomic SAFB1 clone and hybridized to EcoRI-digested genomic DNA. Five independent ES clones containing the targeted mutation of SAFB1 were injected into C57BL/6J blastocysts and transferred to pseudopregnant females. Two lines of SAFB1$^{-/-}$ mice were generated, which were analyzed in a C57BL/6J × 129/Sv mixed genetic background. The mice used in this study were maintained in a pathogen-free facility at BCM. Mice were maintained on a 12-h daylight cycle and fed a diet of a standard food and water ad libitum.

RT-PCR. Total RNA was extracted from frozen organs with TRIzol (Ambion). First-stand cDNA was generated by reverse transcription of 0.5 μg of RNA with a SuperScript II RNase H reverse transcriptase kit (Gibco) and random hexamer oligonucleotides (Gibco). PCR was subsequently performed with a *Taq* polymerase PCR kit (Promega). SAFB1 cDNA spanning exons 10 through 14 was amplified with primers 5′-GCACAAGACTGAGCTGCATGGCAA-3′ and 5′-GGCTGGCTGACTTCCGGTCCTGACTTTTGGAGG-3′. The SAFB1 partial cDNA spanning exons 3 through 5 was amplified with primers 5′-TGGGGAT GGGCAGGAGGATGTGGAG-3′ and 5′-ATGGTGAAGTCAGATGATGAC GT-3′. To analyze IGF1 expression in the liver, we performed reverse transcriptase PCR (RT-PCR) with 5′-GGACCAGAGACCCTTTGCGGGG-3′ and 5′-G GCTGCTTTTGTAGGCTTCAGTGG-3′ (23). As a control, we RT-PCR amplified β-actin with primers 5′-GGAAACCAGGTTGTCAGTC-3′ and 5′-A ACAGAACTTAGGACGAGGG-3′. The PCR conditions used were 95°C for 5 min, 95°C for 30 s, 55°C for 30 s, and 72°C for 30 s, with steps 2 to 4 repeated for 25 cycles. To more precisely measure the relative SAFB1 mRNA expression levels in different mouse tissues, we performed quantitative PCR (qPCR) on an ABI PRISM 7500 sequence detection system (PE Applied Biosystems). Briefly, 1 μg of RNA was reverse transcribed in accordance with standard protocols. One microliter of the diluted cDNA was amplified with 1× SYBR green PCR master mix and 150 nM forward (GAAGAAGCGGAACCTCGACTC) and reverse (TCATCAGGATTCCCACCTTCA) primers for 40 cycles of 95°C for 12 s and 60°C for 1 min. The change in expression was calculated by the ΔΔ Ct method (19, 34) with β-actin (forward primer, CAAGTGCTTCTAGGCGGACTG; reverse primer, AGCCATGCCAATGTTGTCTCT) as an internal control.

Immunoblot analysis. Tissue was crushed, lysed in 5% sodium dodecyl sulfate (SDS), and sonicated. Proteins (50 μg) were resolved by SDS–6% polyacrylamide gel electrophoresis and transferred to nitrocellulose membranes. The membranes were blocked in phosphate-buffered saline (PBS)–0.1% Tween 20 (PBST) plus 5% milk for 1 h at room temperature. SAFB1 primary antibody was diluted 1:1,000 in PBST plus 5% milk and applied to the membranes, which were incubated for 1 h. After washing, the protein-antibody complexes were detected with horseradish peroxidase-linked secondary anti-rabbit antibody (Amersham Biosciences) diluted 1:1,000 in PBST plus 5% milk. The membranes were then washed five times for 5 min each time in PBST, and the signal was developed by enhanced chemiluminescence (Pierce) in accordance with the manufacturer's instructions.

Rabbit SAFB1 antiserum was raised with the N-terminal peptide EGEMKELPEQLQEHAIED, which corresponds to aa 168 to 185 in human SAFB1 (Invitrogen). This peptide is 77% homologous (14 of 18 aa) and 93% similar (17 of 18 aa) to the corresponding mouse SAFB1 peptide, and the antiserum does recognize mouse SAFB1. The antiserum was purified with an A/G protein column (Pierce).

Fertility analysis. To analyze male fertility, wild-type females were mated with SAFB1$^{+/+}$, SAFB1$^{+/-}$, and SAFB1$^{-/-}$ males. To induce superovulation, 6-week-old C57BL/6J females were injected intraperitoneally with 4 U of pregnant mare serum gonadotropin/gestyl (Professional Compounding Center of America) and, after 48 h, 5 U of human CG/pregnyl (Organon Inc.). Females were mated with males, and pregnancy was determined by the presence of a plug.

To analyze female fertility, SAFB1$^{-/-}$, SAFB1$^{+/-}$, and SAFB1$^{+/+}$ females were mated with wild-type males. Females were sacrificed on day 3.5 of pregnancy after 1 p.m. Embryos were isolated from oviducts and uteri, and the number of embryos in each organ was calculated.

Analysis of follicles in ovaries and ovarian transplantation. Reciprocal ovarian transplantation was performed with pairs of 6-week-old littermates as described by Leonardsson et al. (28). Donor and recipient mice were anesthetized with 0.2 ml of Avertin (Sigma). After the ovaries from knockout or wild-type mice were transplanted into wild-type recipients, the skin incisions were closed and the mice were given appropriate postoperative care. The mice were allowed to mate with wild-type males 3 to 4 weeks after surgery.

To count follicles, ovaries were fixed in 4% paraformaldehyde, paraffin embedded, and serially sectioned (5-μm sections at 25-μm intervals). For each ovary, 10 sections were stained with hematoxylin and eosin (H&E), and primordial, primary, and secondary follicles were counted as previously described (41, 45).

Hormone measurements. Blood was collected by cardiac puncture under anesthesia with 0.5 ml of Avetrin IP (Sigma), and serum was stored at −70°C until assayed for hormones. To measure testosterone, estrogen, and progesterone levels, ^{125}I radioimmunoassay kits were used in accordance with the manufacturer's (Diagnostic Systems Laboratories) protocols. IGF1 was measured with enzyme-linked immunosorbent assay kits in accordance with the manufacturer's (Diagnostic Systems Laboratories) protocol.

Skeletal analysis. Newborns were euthanized by CO_2 asphyxiation, and as much skin and muscle as possible was removed. After the body was eviscerated through midline abdominal incision, the carcasses were fixed in ethanol at room temperature for 1 day. The skeletons were stained with alcian blue 8GX (Sigma) and alizarin red S (Sigma) as previously described (35).

Histological analysis. Tissues isolated from mice were fixed in fresh 4% paraformaldehyde overnight at 4°C. The testes were fixed in Bouin's solution. Excess fixative was removed with 70% ethanol. Tissues were then embedded in paraffin, sectioned (5 μm), and H&E stained by a standard protocol. To measure apoptosis, a terminal deoxynucleotidyltransferase-mediated dUTP-biotin nick end labeling staining kit (Roche) was used. To analyze the number and position of germ cells, anti-germ cell nuclear antigen 1 (GCNA-1) antibody was diluted 1:1,000 as previously described (16) and visualized with goat anti-rat secondary antibody (Jackson ImmunoResearch Laboratories, Inc.). To determine the num-

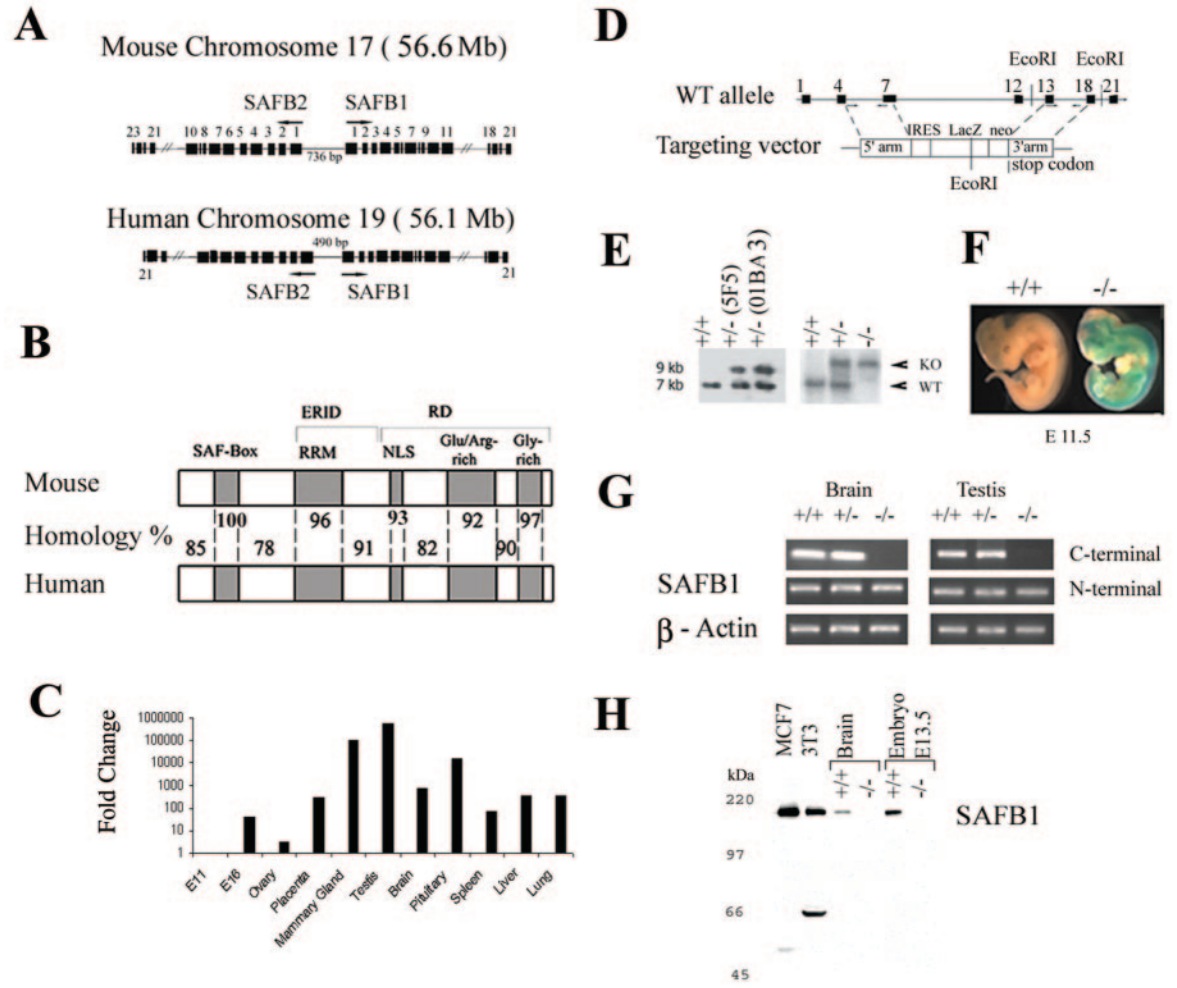

FIG. 1. Generation of SAFB1 knockout mice by homologous recombination. (A) The mouse and human genes for SAFB1 and SAFB2 lie adjacent to each other in a head-to-head orientation and are separated by a small intragenic region. (B) Structure of the gene for SAFB1 and similarity between human and mouse orthologues. Functional protein domains include the SAF-Box, RRM, NLS, ERα interaction domain (ERID), and RD. Percent similarities between the human and mouse proteins are indicated. (C) mSAFB1 expression as detected by real-time qPCR with tissues from adult C57BL/6J × 129/Sv mice and embryos (as indicated). The change was calculated by the ΔΔ Ct method, where SAFB1 mRNA levels are presented as the change in gene expression normalized to β-actin and relative to SAFB1 expression levels in E11. The bars represent averages from triplicate measurements. (D) Structure of the wild-type (WT) allele and the targeting vector. Mouse SAFB1 exons are indicated by black boxes. Homologous recombination results in the replacement of exons 7 to 13 with a cassette including an IRES and a *lacZ-neo* gene fusion. (E) Detection of genotypes with DNA from ES cells (left side) and from tails (right side) by Southern blot analysis. Genomic DNA was digested with EcoRI and probed with a 700-bp 3′ external probe that detects a 7-kb wild-type allele and a 9.7-kb null (knockout [KO]) allele. 5F5 and O1BA3 are independent ES cell lines that resulted in germ line transmission. (F) Whole-mount β-galactosidase staining of embryos at E11.5. (G) RT-PCR analysis with primers specific for C-terminal SAFB1 (388 bp), N-terminal SAFB1 (275 bp), and β-actin (267 bp). (H) Immunoblot analysis verifies not only the absence of full-length SAFB1 protein in extracts from SAFB1$^{-/-}$ brains and embryos but also the lack of a potential small truncated product. Extracts from NIH 3T3 fibroblasts and human MCF-7 cell lines served as positive controls.

ber of blood vessels, rat anti-mouse CD31 monoclonal antibody (BD Biosciences) was used at a concentration of 1:1,000 as previously described (48).

The *lacZ* expression in the embryos was assessed by performing β-galactosidase (5-bromo-4-chloro-3-indolyl-β-D-galactopyranoside [X-Gal]) staining. Whole embryos were fixed in 2% paraformaldehyde in PBS at 4°C for 20 min. LacZ staining was performed as previously described (6).

Analysis of transcription and signaling in MEFs. To generate mouse embryonic fibroblasts (MEFs), we isolated littermate embryos from pregnant mothers at 12.5 days postcoitus (dpc). Embryonic tissue without organs was washed in PBS, minced, digested in 0.25% trypsin–0.5 mM EDTA, and seeded in high-glucose Dulbecco modified Eagle medium supplemented with 10% fetal bovine serum, 100 U of penicillin per ml, 100 μg of streptomycin per ml, and sodium pyruvate. The MEFs were immortalized by the standard 3T3 protocol, in which 300,000 cells were reseeded every 3 days. To analyze IGF1 signaling, immortalized MEFs (passage 35) were maintained in 10% serum overnight and switched to serum-free medium for 18 to 24 h, and then IGF1 (100 ng/ml) was added and the mixture was incubated for 15 min. Whole-cell SDS extracts were subjected to SDS-polyacrylamide gel electrophoresis and immunoblotted for p-IRS1 and p-IGF1R (Biosource) as previously described (27). To measure ERα transcriptional activity, we performed reporter assays as previously described (39, 47). Briefly, primary or immortalized MEFs were plated in six-well plates, transfected with 25 ng of ERα and 500 ng of ERE-Tk-Luc, switched to charcoal-stripped serum, treated as indicated in the figure legends, and assessed for relative luciferase units.

Statistical analysis. Chi-square or exact tests for goodness of fit were used to evaluate agreement of the observed genotype distribution with a Mendelian ratio of 1:2:1. In order to compare distributions of genotypes across different factors (e.g., male versus female, days of development), a log-linear model was fitted to

TABLE 1. Numbers and frequencies of wild-type and SAFB1 mutant pups in litters of SAFB1$^{+/-}$ intercrosses in 01BA3 and 5F5 lines

Line and no. of offspring	No. that were:			+/+:+/−:−/− ratio	*P* value based on:	
	+/+	+/−	−/−		Chi-square test[a]	Likelihood ratio test[b]
O1BA3						
Total, 816	323	431	62	1:1.3:0.19	<0.0001	
Females, 430	180	223	27	1:1.2:0.15	<0.0001	0.180
Males, 386	143	208	35	1:1.5:0.24	<0.0001	
5F5						
Total, 638	250	347	41	1:1.4:0.16	<0.0001	
Females, 318	134	163	21	1:1.2:0.16	<0.0001	0.274
Males, 320	116	184	20	1:1.6:0.17	<0.0001	

[a] Chi-square test for goodness of fit to compare the observed distribution of genotypes with the Mendelian 1:2:1 ratio.
[b] Likelihood ratio test comparing distribution of genotype between females versus males from a log-linear model.

the observed counts. Descriptive statistics were calculated to summarize different study parameters, including number of pups, number of embryos, testosterone and estradiol levels, serum IGF1 levels, and body weight. Tests of normality were performed on these parameters prior to implementation of parametric statistical testing (two-sample *t* tests and growth curve models). Nonparametric methods, specifically, Wilcoxon rank-sum tests, were used in place of the two-sample *t* test when normality assumptions were violated or in experiments with small sample sizes. Finally, growth curve models were fitted on body weight measurements over time to estimate and compare slopes across different genotypes. Adjusted *P* values obtained with the Holms procedure were calculated to account for multiple pairwise comparisons with the wild-type group.

RESULTS

Generation of SAFB1 knockout mice. Mouse SAFB1 genomic DNA was isolated from a 129/Sv phage genomic library and used for fluorescence in situ hybridization analysis, which identified chromosome 17C as its single locus (data not shown). The mouse gene for SAFB1 has a total length of 20.97 kb, consists of 21 exons, and as in the human genome, maps adjacent to its paralogue SAFB2 (Fig. 1A). There is high similarity between the mouse and human SAFB1 orthologues, as depicted in Fig. 1B. Functional domains such as the SAF-Box, RRM, and NLS have homologies of 100, 96, and 93%, respectively. The ERα interaction domain and the repression domain (RD) are also highly conserved between the mouse and human SAFB1 proteins, showing homologies of 93 and 91%, respectively. To analyze expression of SAFB1 in mice, we performed real-time qPCR assays with a number of tissues. As shown in Fig. 1C, SAFB1 is ubiquitously expressed in both hormone-dependent and -independent adult tissues, with the highest expression levels in the testes, mammary glands, and brain. We have also analyzed expression during various stages of embryonic development as early as embryonic day 8 (E8) and have detected SAFB1 mRNA expression (Fig. 1C and data not shown).

To investigate the physiological role of SAFB1, we created mutant mice by homologous recombination in 129/Sv ES cells as outlined in Fig. 1D. We sought to disrupt the ERα interaction domain and RD and therefore replaced exons 7 to 13 with a cassette containing an IRES and a *lacZ* (β-galactosidase)-*neo* gene fusion. The targeting construct was linearized and electroporated into ES cells. Homologous recombination was screened by Southern blot analysis (Fig. 1E, left side). Five recombinant clones were injected into C57BL/6 blastocysts, and two (5F5 and 01BA3) were transmitted to germ line. Heterozygous F_1 mice (SAFB1$^{+/-}$) from each clone (5F5 and 01BA3) were intercrossed to produce two independent lines of homozygous mutant mice (SAFB1$^{-/-}$). The genotype was confirmed by Southern blot analysis (Fig. 1E, right side). Additionally, we confirmed *lacZ* expression by X-Gal staining in postimplantation SAFB1$^{-/-}$ embryos at E11.5. As shown in Fig. 1F, *lacZ* was ubiquitously expressed, except in the heart.

To verify loss of SAFB1 expression, we performed RT-PCR assays with primers spanning exons 10 through 14. As expected, these primers amplified a 388-bp product from SAFB1$^{+/+}$ and SAFB1$^{+/-}$ mice but not from SAFB1$^{-/-}$ mice (Fig. 1G). We also examined potential transcripts that could be generated from the remaining SAFB1 exons (1 through 6). Primers located in exons 3 and 5 amplified a 275-bp product from SAFB1$^{-/-}$ tissues, indicating that the mutated SAFB1 allele can generate an mRNA transcript. To analyze whether this transcript could result in the generation of a truncated SAFB1 protein, we raised polyclonal antibodies against the N terminus of human SAFB1 (which also cross-reacted with mouse SAFB1), and these were used for immunoblotting. We were unable to detect any protein in SAFB1$^{-/-}$ mice (Fig. 1H), even after prolonged exposure of the film, suggesting that any potential truncated protein is highly unstable. Thus, our model represents a true SAFB1 null mutation.

Since the genes for SAFB1 and SAFB2 are clustered together and, at least in humans, their transcription is driven by a bidirectional promoter (46), we also analyzed expression of SAFB2 to confirm that the knockout was specific for SAFB1. RT-PCR analysis revealed that SAFB2 expression was not reduced (data not shown). We therefore concluded that we had generated two independent lines of SAFB1$^{-/-}$ mice without simultaneously disrupting expression of SAFB2.

Pre- and postnatal lethality of SAFB$^{-/-}$ mice. SAFB1$^{+/-}$ intercrosses produced SAFB1$^{-/-}$ and SAFB1$^{+/-}$ progeny that were recovered at less than the predicted Mendelian distribution in both lines (5F5 and 01BA3) for both males and females ($P < 0.0001$) (Table 1). Only 103 of 1,454 live births from 248 litters were homozygotes, a loss of 83%. No statistically significant difference in genotype distribution was observed between males versus females in the 01AB3 or 5F5 line, as shown in Table 1. Interestingly, we also noted a reduction (32%) in the

TABLE 2. Two different time points of lethality in SAFB1$^{-/-}$ mice[a]

Time of development	Observed no. of SAFB1$^{-/-}$ mice total no.	Ratio of SAFB1$^{-/-}$ mice to total no.	*P* value[b] (exact 95% CI)
E10.5	8/48	0.167	0.238 (0.07, 0.30)
E11.5–16.5	15/87	0.172	0.114 (0.10, 0.27)
E18.5	5/34	0.147	0.228 (0.05, 0.31)
1 dpp	18/114	0.158	0.025 (0.10, 0.24)
4–6 dpp	2/51	0.039	0.0001 (0.005, 0.13)

[a] Embryos (E10.5 to E18.5) and newborn pups (1 to 6 dpp) were genotyped, and the number of SAFB1$^{-/-}$ mice is listed in relation to the total number of mice analyzed at each time point.

[b] Calculations of *P* values were based on the exact test for goodness of fit to compare the observed distribution of the SAFB1$^{-/-}$ genotype with the expected Mendelian ratio of 0.25. CI, confidence interval.

expected number of SAFB1$^{+/-}$ progeny, suggesting haploinsufficiency problems, at least during embryonic development.

To understand the reason for the non-Mendelian distribution of progeny from SAFB1$^{+/-}$ intercrosses, we carefully examined genotype distribution from E10.5 until 1 to 6 days postpartum (dpp) (Table 2). Genotyping demonstrated reduced SAFB1$^{-/-}$ embryo number at E10.5, although this did not reach statistical significance ($P = 0.238$). There was no additional reduction between E10.5 and E18.5. Among the newborn SAFB1$^{-/-}$ pups at 1 dpp, there was a statistically significant reduction from the expected Mendelian ratio of 0.25. At 4 to 6 dpp, a further decline in the number of SAFB1$^{-/-}$ pups was observed. To examine the dramatic loss of SAFB1$^{-/-}$ pups following birth, we visually monitored 233 newborns during their first 3 days after birth. We observed that 14 newborns (6%) died at 1 dpp and 22 (9.4%) died during the next 2 days. Genotyping of the dead pups ($n = 36$) showed that 32 (88%) were SAFB1$^{-/-}$. In summary, deletion of SAFB1 resulted in prenatal and significant neonatal lethality.

The newborn SAFB1$^{-/-}$ mice were characterized by cyanotic skin and small size (Fig. 2A). In contrast to their wild-type littermates, no milk was observed in their stomachs. This could represent a direct suckling defect. However, since pups have to hold their breath while suckling milk, these observations could also indicate anemia and dysfunctional oxygen exchange. In support of this hypothesis, SAFB1$^{-/-}$ embryos showed incomplete maturation of the alveoli in the lungs and fewer erythrocytes in the liver (Fig. 2B), which is the site of embryonal hematopoiesis. This was further confirmed through staining of blood vessels with CD31 antibodies, which detected a lower number of blood vessels in three out of five SAFB1$^{-/-}$ livers compared to their wild-type littermates. A representative of the three SAFB1$^{-/-}$ livers is shown in Fig. 2C.

In summary, we observed partial lethality in both SAFB1$^{-/-}$ and SAFB1$^{+/-}$ mice. SAFB1$^{-/-}$ mice die at two time points: before E10.5 and within the first days of life. While we do not know the exact cause of death, our data suggest that it may result from incomplete development of the lungs and the hematopoietic system.

SAFB1 loss is associated with growth retardation and low circulating IGF1 levels. SAFB1$^{-/-}$ mice could be easily distinguished from their wild-type littermates by their smaller size (Fig. 3A). At 3 weeks of age, the difference in weight between

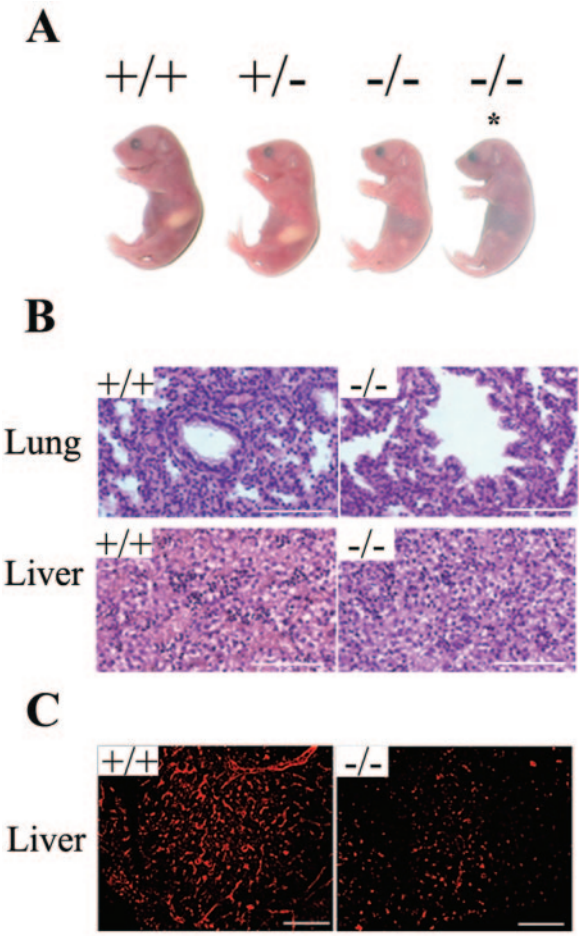

FIG. 2. Defects in lung maturation and hematopoietic system development in SAFB1$^{-/-}$ mice. (A) SAFB1$^{+/+}$, SAFB1$^{+/-}$, and SAFB1$^{-/-}$ newborn pups on the first day after birth at 8 a.m. Lack of milk is obvious in the stomachs of SAFB1$^{-/-}$ pups. A dead SAFB1$^{-/-}$ newborn is marked by an asterisk. (B) H&E-stained lung and liver sections (E19). The pictures are representative of two animals analyzed per genotype. (C) Sections from SAFB1$^{+/+}$ and SAFB1$^{-/-}$ livers (E19) were stained with CD31 antibody to visualize blood vessels. Bars, 100 μm.

SAFB1$^{-/-}$ mice and their wild-type littermates was 45% for males ($P < 0.0001$) and 30% for females ($P = 0.001$) (Fig. 3B). In contrast, there was no growth defect in the SAFB1$^{+/-}$ mice. The weight difference between SAFB1$^{+/+}$ and SAFB1$^{-/-}$ pups remained constant during pubertal growth, suggesting that the growth deficit at birth probably resulted from in utero growth retardation. Supporting this, SAFB1$^{-/-}$ embryos were almost 20% smaller than their SAFB1$^{+/+}$ littermates ($P = 0.0032$), starting at E15 (Fig. 3C).

To examine whether the decrease in size and weight was reflected in a smaller overall skeleton, we analyzed skeletal growth in SAFB1$^{+/+}$ and SAFB1$^{-/-}$ newborns by measuring the skulls (no. 1 and 2), the width of the thorax (no. 3), and the length of the spine from the first vertebra to the vertebra of the pelvis (no. 4) (Fig. 3D). Analysis of data from seven SAFB1$^{-/-}$ mice and their SAFB1$^{+/+}$ littermates revealed a statistically significant decrease in the size of the entire skeleton, with the most pronounced effect in the thorax (Fig. 3E).

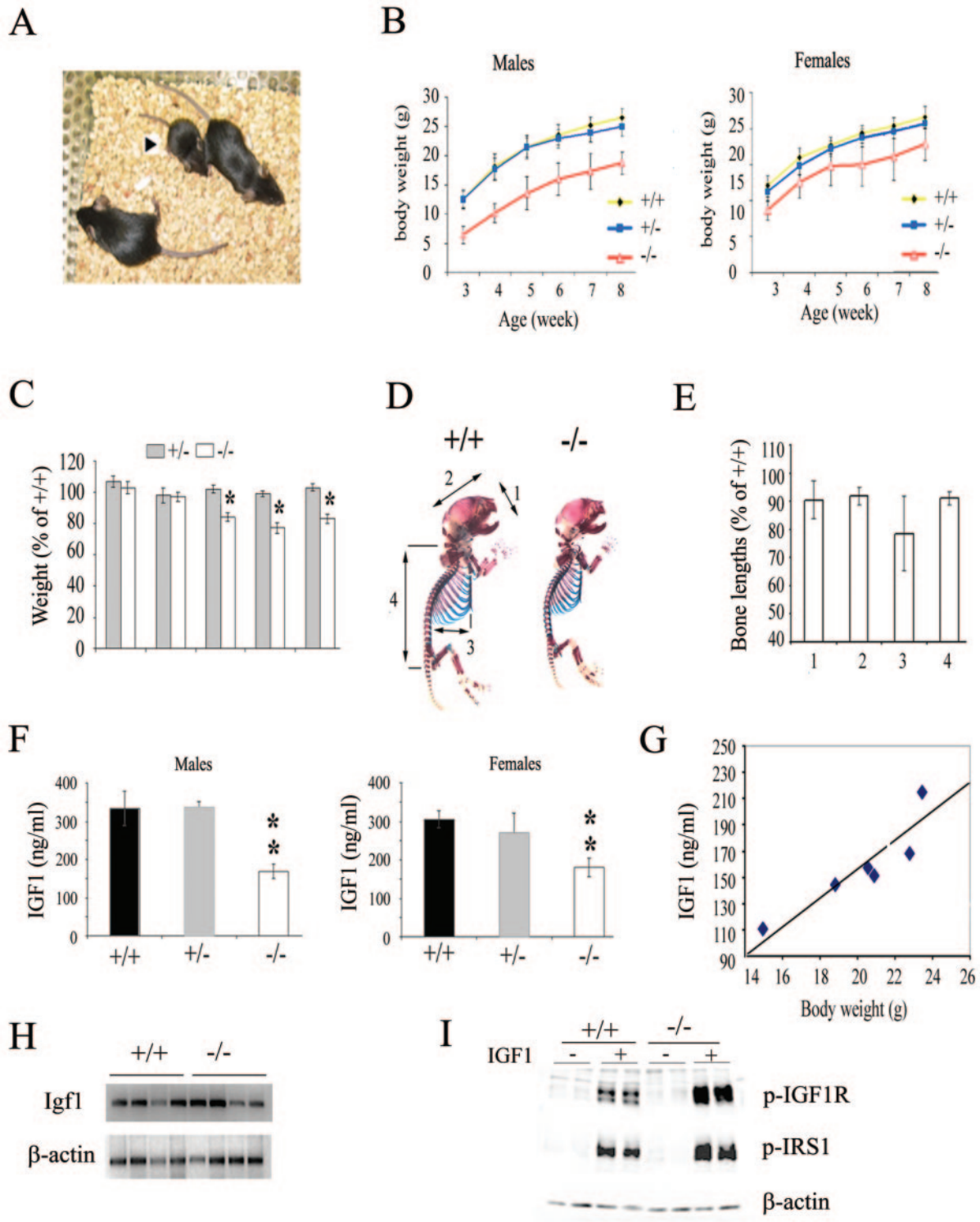

FIG. 3. Growth defects of SAFB1$^{-/-}$ mice. (A) Six-week-old SAFB1$^{-/-}$ (arrow), SAFB1$^{+/-}$, and SAFB1$^{+/+}$ female mice. (B) Growth curves were generated by weighing 14 male and 12 female mice of each genotype weekly. There was a significant decrease in the weights of SAFB1$^{-/-}$ mice when we used a longitudinal model based on comparison of SAFB1$^{-/-}$ males ($P < 0.0001$) and females ($P = 0.001$) with SAFB1$^{+/+}$ males and females, respectively. (C) Body weights of embryos (E11 and E14, $n = 7$ per genotype; E15, $n = 5$ per genotype) and newborn pups (1 and 2 dpp, $n = 19$ per genotype). Data are presented as percent weight of SAFB1$^{+/-}$ (gray bars) and SAFB1$^{-/-}$ (white bars) mice relative to that of SAFB1$^{+/+}$ mice (mean ± SD). Asterisks indicate P values based on t test for pairwise comparison between SAFB1$^{+/-}$ and SAFB1$^{-/-}$ versus SAFB1$^{+/+}$ that indicated significant differences for SAFB1$^{-/-}$ mice on E15 ($P = 0.0001$), 1 dpp ($P < 0.0001$), and 2 dpp ($P = 0.0018$). Testing of data for normality indicated no significant departure from the assumption of normality. (D) Representative pictures of SAFB1$^{+/+}$ and SAFB1$^{-/-}$ newborn skeletons with arrows indicating positions of measurements. (E) The bars present percentages of bone lengths (mean ± standard deviation) from SAFB1$^{-/-}$ newborns relative to those of SAFB1$^{+/+}$ newborns ($n = 7$ per genotype, pooled from four offspring). Testing

TABLE 3. Infertility in SAFB1$^{-/-}$ males and subfertility in SAFB1$^{-/-}$ females[a]

Genotype (males × females)	No. of males	No. of females	No. (%) of pregnant females	*P* value (Fisher's exact test)[b]	Avg no. of pups/litter ± SD	*P* value (*t* test)[c]
+/+ × +/+	2	5	5 (100)		5.6 ± 1.52	
+/− × +/+	6	11	10 (91)	0.99	6.1 ± 1.70	0.999
−/− × +/+	7	13	0	0.0005	NA[d]	
+/+ × +/−	5	11	11 (100)		6.4 ± 1.86	0.999
+/+ × −/−	3	14	5 (36)	0.032	3.2 ± 0.45	0.086

[a] Breeding pairs were set up as indicated. The proportion of pregnant females was statistically significantly lower in the −/− × +/+ or +/+ × −/− genotype compared to the +/+ × +/+ breeding pairs ($p = 0.0005$ and 0.032, respectively). (A *P* value cannot be generated when comparing the +/+ × +/− breeding pair to the wild-type breeding pair since all of the females in this group were pregnant and therefore there is no distribution of pregnant versus nonpregnant in both comparison groups.) There was an indication of a reduction in the average number of pups from the +/+ × −/− compared to the +/+ × +/+ breeding pair. This comparison did not achieve statistical significance because of the small numbers.

[b] *P* value from Fisher's exact test for comparisons with the +/+ × +/+ breeding pair.

[c] *P* value from a two-sample *t* test with Holm's adjustment for multiple comparisons with the +/+ × +/+ breeding pair.

[d] NA, not applicable.

IGF1 is an important regulator of embryonic and postpartum growth. We therefore measured serum IGF1 levels in 3- to 4-month-old SAFB1$^{+/+}$, SAFB1$^{+/-}$, and SAFB1$^{-/-}$ mice. SAFB1$^{-/-}$, but not SAFB1$^{+/-}$, mice had significantly lower serum IGF1 levels than did SAFB1$^{+/+}$ mice, independently of the sex of the mice (Fig. 3F). Statistical analysis revealed a tight correlation between the serum IGF1 levels and body weights of individual SAFB1$^{-/-}$ mice (Fig. 3G), suggesting that the serum IGF1 deficiency could, at least in part, account for the growth retardation of the SAFB1$^{-/-}$ mice.

The main source of circulating IGF1 is growth hormone-induced secretion of IGF1 from the liver. To analyze whether the decreased serum IGF1 levels resulted from a defect in IGF1 production, we measured liver IGF1 mRNA levels in wild-type and SAFB1$^{-/-}$ mice. We did not detect any significant differences in IGF1 mRNA levels (Fig. 3H), suggesting that the observed decrease in serum IGF1 levels may reflect a decreased half-life of circulating IGF1, possibly because of changes in IGF-binding protein expression. Preliminary studies have indicated that IGF-binding protein 3 and 6 levels are lower in SAFB1$^{-/-}$ mice (data not shown).

SRC3$^{-/-}$ mice also have low serum IGF1 levels, and MEFs from these mice show a diminished response to IGF1 signaling, growth, and migration (26, 50). We therefore generated immortalized wild-type and SAFB1$^{-/-}$ MEFs and analyzed proliferation and IGF1 signaling (Fig. 3I). Growth curves of early-passage SAFB1$^{+/+}$ and SAFB1$^{-/-}$ MEFs did not reveal any significant differences in growth (data not shown). Paradoxically, while SAFB1$^{-/-}$ mice are small and have low circulating IGF levels, SAFB1$^{-/-}$ MEFs showed increased IGF1 receptor phosphorylation in response to IGF1. Supporting this observation, the same cells also showed increased phosphorylation of IRS1, an adaptor that is immediately downstream of the IGF1 receptor. Immunofluorescence detection of IRS1 revealed mainly cytoplasmic staining and some nuclear localization; however, there was no difference between wild-type and null MEFs. Thus, SAFB1 deletion results in a number of defects in the IGF1 system, including both systemic and cell-intrinsic changes.

SAFB1 is required for normal male reproductive function. Regular breeding of SAFB1$^{-/-}$ males with wild-type females failed to result in pregnancy, whereas breeding of SAFB1$^{+/-}$ males did (Table 3 and data not shown). The sterility of SAFB1$^{-/-}$ males was further confirmed through controlled breeding experiments in which four males of each genotype were bred with superovulated C57BL/6 females. In this experiment, only one out of four SAFB1$^{-/-}$ males bred, as judged by the presence of vaginal plugs in the females on the next morning, suggesting a lack of sex drive. In contrast, breeding of all SAFB1$^{+/-}$ and SAFB1$^{+/+}$ mice resulted in plug formation in the superovulated females. To determine whether fertilization had occurred, the oviducts of the females were flushed 1 day after breeding, and two-cell embryos and oocytes were counted. After breeding with SAFB1$^{-/-}$ males, all superovulated females ($n = 9$) showed only nonfertilized oocytes and no two-cell embryos in their oviducts. In contrast, all oviducts from females crossed with SAFB1$^{+/-}$ and SAFB1$^{+/+}$ males contained two-cell embryos along with oocytes.

The overall reproductive systems of SAFB1$^{-/-}$ males were very small (Fig. 4A). SAFB1$^{-/-}$ mice were hypogonadal—the paired testicular weight was reduced by approximately 80% (25 ± 5 mg) in comparison with that of SAFB1$^{+/+}$ males (120 ± 20 mg) (Fig. 4B) after correction for the decreased body weight of SAFB1$^{-/-}$ males. Since hypogonadism and sterility are known to be associated with low steroid levels, we measured serum testosterone levels and found that they were signifi-

of data for normality indicated a significant departure from the assumption of normality, so the nonparametric Wilcoxon signed-rank test was used instead of the paired *t* test. The Wilcoxon signed-rank paired test revealed that all skeleton measurements of SAFB1$^{-/-}$ mice were significantly smaller than those of SAFB1$^{+/+}$ mice ($P = 0.0078$). (F) Serum IGF1 levels were measured in 3- to 4-month-old male and female mice ($n = 5$ per group), and bars represent the mean ± the standard deviation. Two-sample *t* tests with Holms adjustment for multiple comparisons of SAFB1$^{+/-}$ and SAFB1$^{-/-}$ mice with the SAFB1$^{+/+}$ group showed significantly lower IGF1 levels in SAFB1$^{-/-}$ mice, independent of sex ($P = 0.01$). Testing of data for normality indicated no significant departure from the assumption of *t*-test normality. (G) Significant correlation between IGF1 levels and body weight in SAFB1$^{-/-}$ mice ($r^2 = 0.914$, $P < 0.005$). (H) Semiquantitative RT-PCR analysis of liver mRNA with specific primers for IGF1 and β-actin. (I) IGF1 signaling was analyzed by incubating immortalized MEFs from SAFB1$^{+/+}$ and SAFB1$^{-/-}$ littermate embryos for 18 h in serum-free medium, adding 100 ng of IGF1 per ml, incubating the mixture for 15 min, harvesting whole-cell SDS extracts, and immunoblotting with antibodies as indicated.

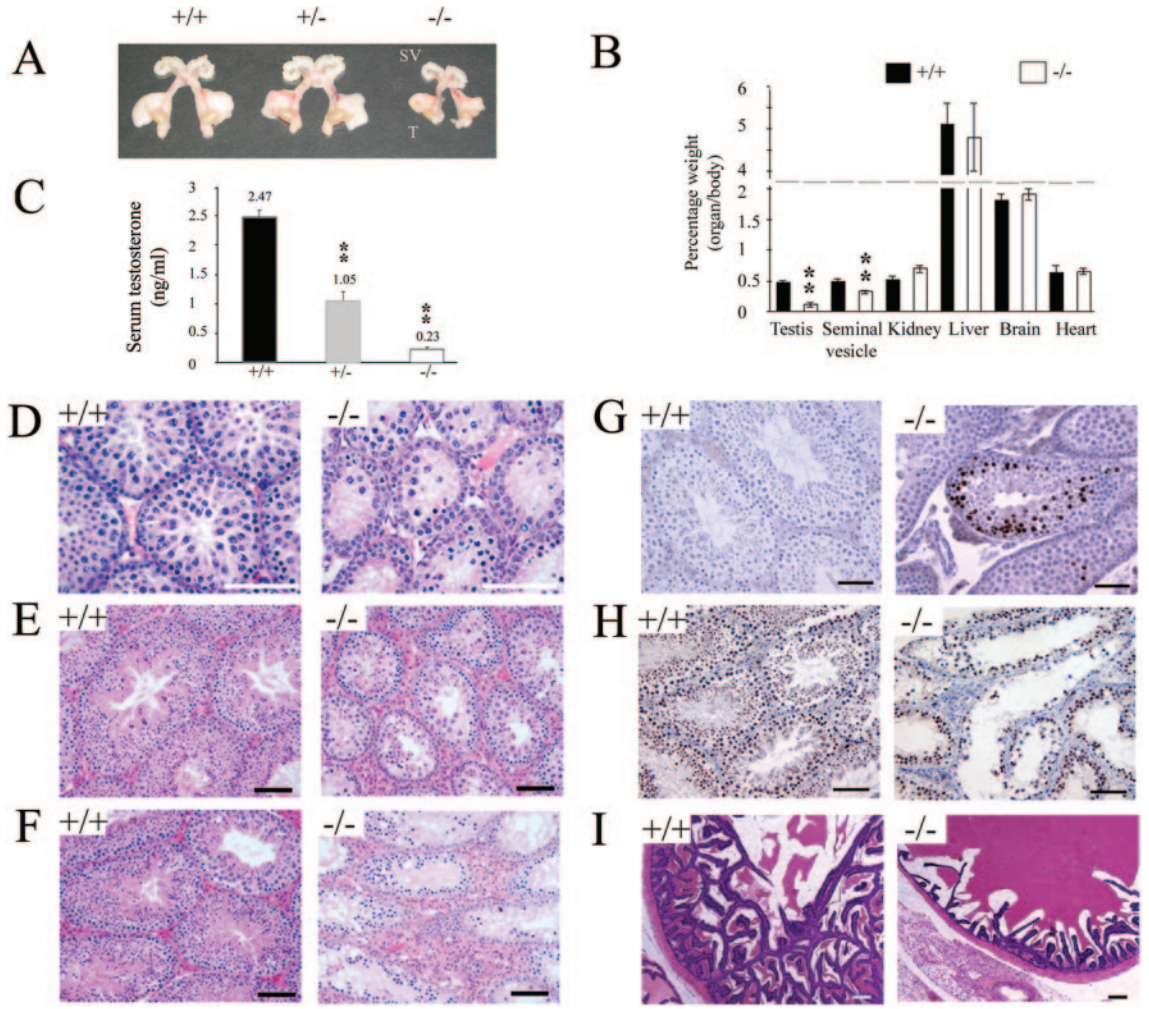

FIG. 4. Sterility of SAFB1$^{-/-}$ males. (A) Reproductive tracts of SAFB1$^{+/+}$, SAFB1$^{+/-}$, and SAFB1$^{-/-}$ male mice at 3 months of age, including the testes (T) and seminal vesicles (SV). (B) Testosterone was measured in serum samples from 3-month-old SAFB1$^{+/+}$, SAFB1$^{+/-}$, and SAFB1$^{-/-}$ male mice ($n = 9$ mice per genotype), and results are shown as the mean ± the standard deviation. A two-sample t test was used to calculate P values (SAFB1$^{+/-}$, $P = 0.0001$; SAFB1$^{-/-}$, $P < 0.0001$). (C) Weights of organs from 3-month-old SAFB1$^{+/+}$ and SAFB1$^{-/-}$ males ($n = 9$ per genotype) are presented as percent organ weight corrected for total body weight (mean ± standard deviation). The testes and seminal vesicles of SAFB1$^{-/-}$ males are significantly smaller ($P < 0.0001$), whereas other organs are in proportion with their lower overall body weight. (D to F) H&E staining of testes from SAFB1$^{+/+}$ and SAFB1$^{-/-}$ males. Representative pictures of testes from 3-week-old ($n = 3$ per genotype) (D), 3-month-old ($n = 4$ per genotype) (E), and 9-month-old ($n = 3$ per genotype) (F) males are shown. (G) Increased apoptosis in SAFB1$^{-/-}$ mouse testes, as measured by terminal deoxynucleotidyltransferase-mediated dUTP-biotin nick end labeling staining (brown-staining cells). Testes from three mice per genotype were analyzed, and representative pictures are shown. (H) Testis sections from 9-month-old males ($n = 2$ per genotype) were stained with anti-GCNA-1 antibodies, and representative pictures are shown. (I) H&E staining of seminal vesicles from SAFB1$^{+/+}$ and SAFB1$^{-/-}$ males. Representative pictures of seminal vesicles from 3-month-old males ($n = 4$ per genotype) are shown. Bars in panels D to I, 100 μm.

cantly decreased in SAFB1$^{-/-}$ and SAFB1$^{+/-}$ males (Fig. 4C). We also measured serum estradiol levels and did not detect any significant difference among the different genotypes (data not shown).

Not surprisingly, detailed analysis of the testes revealed several defects (Fig. 4D to H). Already in 3-week-old males, the seminiferous tubules contained fewer germ cells (Fig. 4D). Mature testes from 3-month-old SAFB1$^{-/-}$ males demonstrated an arrest of spermatogenesis (Fig. 4E), which was confirmed by showing that spermatozoa were absent in SAFB1$^{-/-}$ epididymides (data not shown). Leydig cell hyperplasia was observed, a phenotype that was even more severe in older mice (Fig. 4F), in which Leydig cell hyperplasia and tubular degeneration affected the majority of the testes. The testicular tubular degeneration was associated with increased apoptosis of germ cells in SAFB1$^{-/-}$ tubules (Fig. 4G). To determine whether loss of germ cells had already begun during embryogenesis, we stained testes from newborn males with an antibody recognizing GCNA-1. We did not detect any significant differences in the number or position of germ cells between testes from newborn SAFB1$^{+/+}$ and SAFB1$^{-/-}$ mice (data not shown). In contrast, the seminiferous tubules from 9-month-old SAFB1$^{-/-}$ males contained fewer germ cells (Fig. 4H), suggesting that loss of germ cells occurs postnatally. The lack of sperm development is not the result of meiotic defects, since testosterone treatment of the mice can restore germ cell development (Y. K. Lo et al., unpublished data).

We also analyzed the structure of seminal vesicles, since

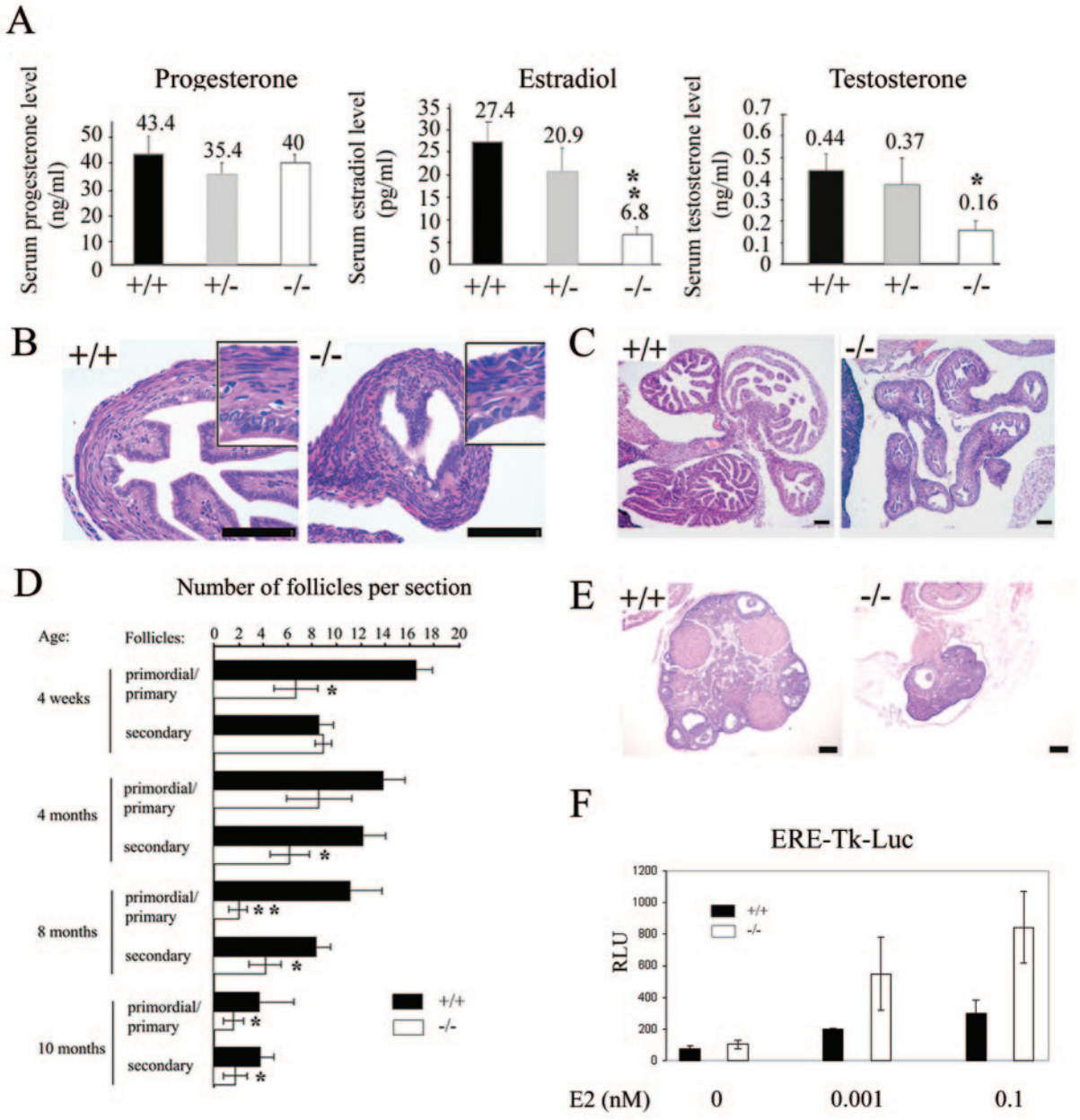

FIG. 5. Dysfunction of the reproductive system in SAFB1$^{-/-}$ female mice. (A) Serum samples were collected from pregnant females at 3.5 dpc and analyzed for progesterone, estradiol, and testosterone ($n = 5$ mice per group). Bars represent means ± standard deviations. Statistical analysis was done with the two-sample t test, and significant differences in estradiol ($P = 0.01$) and testosterone ($P = 0.0042$) levels were seen. (B and C) Representative H&E-stained oviduct sections from 4-week-old virgin SAFB1$^{+/+}$ and SAFB1$^{-/-}$ female mice ($n = 6$ per genotype). Bars, 100 μm. (D) Ovaries of 4-week-old mice ($n = 4$ per genotype) and 4,- 8-, and 10-month-old mice ($n = 1$ per genotype) were step sectioned at 25-μm intervals ($n = 10$). Bars represent means ± standard deviations. (E) H&E-stained ovary sections from 10-month-old SAFB1$^{+/+}$ and SAFB1$^{-/-}$ mice. Bars, 200 μm. (F) Immortalized SAFB1$^{+/+}$ and SAFB1$^{-/-}$ MEFs were transfected with ERE-Tk-Luc and ERα expression plasmids and treated with vehicle only or estradiol as indicated, and relative light units (RLU) were determined. Bars represent means ± standard deviations from triplicate plates.

their growth and function is highly dependent on testosterone. As shown in Fig. 4B, seminal vesicle weights were significantly lower in SAFB1$^{-/-}$ males than in wild-type mice (SAFB1$^{+/+}$, 0.44 ± 0.07 g; SAFB1$^{-/-}$, 0.29 ± 0.075 g). Additionally, the seminal vesicles of SAFB1$^{-/-}$ males also had a more primitive columnar epithelium without branching into secondary and tertiary folds (Fig. 4I), suggesting that SAFB1 loss results in defects in the development of functional seminal vesicles.

In summary, SAFB1$^{-/-}$ males are sterile and show azoospermia, progressive testicular tubular degeneration, increased apoptosis of germ cells, and Leydig cell hyperplasia. These defects are likely to be caused, at least in part, by low levels of testosterone and IGF1 in SAFB1$^{-/-}$ mice.

Multiple fertility abnormalities in SAFB1$^{-/-}$ female mice caused by alterations in hormone levels and cell-intrinsic defects. SAFB1$^{-/-}$ female mice were subfertile, as revealed by

the results of natural mating with wild-type males (Table 3). To determine whether the decreased fertility was due to altered sexual behavior, we bred 15 virgin 6-week-old SAFB1$^{-/-}$, SAFB1$^{+/-}$, and SAFB1$^{-/-}$ females with wild-type males and monitored them for the presence of vaginal plugs. Copulation plugs were detected in 86% (13 of 15) of SAFB1$^{-/-}$ mice, compared with 93% of SAFB1$^{+/-}$ (14 of 15) and SAFB1$^{+/+}$ (14 of 15) mice. This observation suggests that SAFB1$^{-/-}$ female mice do not have reduced sexual behavior and, since mating in mice is associated with ovulation, that the ovaries are functional. Indeed, gross histopathological evaluation of the ovaries at 3.5 days of pregnancy (3.5 dpc) did not identify any major defects in SAFB1$^{-/-}$ mouse ovaries (data not shown). Fully developed corpora lutea could be detected, which were able to secrete progesterone (Fig. 5A). In contrast, serum estradiol (SAFB1$^{+/+}$, 27.4 ± 11.13 pg/ml; SAFB1$^{-/-}$, 6.75 ± 3.59 pg/ml; $P = 0.01$) and testosterone (SAFB1$^{+/+}$, 0.45 ± 0.16 ng/ml; SAFB1$^{-/-}$, 0.16 ± 0.06 ng/ml; $P = 0.042$) levels were significantly decreased in pregnant SAFB1$^{-/-}$ females (Fig. 5A).

To further substantiate our findings of normal ovarian function, we performed ovarian transfer experiments in which ovaries from SAFB1$^{+/+}$ and SAFB1$^{-/-}$ females were transplanted into wild-type host females. These transplantation experiments resulted in similar rates of pregnancy—transplantation of SAFB1$^{-/-}$ and SAFB1$^{+/+}$ ovaries resulted in litters in three out of six and three out of five females, respectively. We thus concluded that the reduced pregnancy in SAFB1$^{-/-}$ females was not due to intrinsic defects but rather to loss of embryos after fertilization.

To examine the latter point further, we analyzed the location of embryos at 3.5 dpc, when they should be found in the uterus. We dissected oviducts and uteri from SAFB1$^{+/+}$, SAFB1$^{+/-}$, and SAFB1$^{-/-}$ females (five per genotype). For the SAFB1$^{-/-}$ mice, we chose females that were unable to develop pregnancy after a first ($n = 2$) or second ($n = 3$) copulation. We flushed out the oviducts and uterus, and as expected, all embryos from SAFB1$^{+/+}$ and SAFB1$^{+/-}$ females were found in the uterus. In contrast, in all SAFB1$^{-/-}$ females the embryos were isolated from the oviduct, suggesting a defect in oviductal transport. Additionally, significantly fewer embryos were recovered from SAFB1$^{-/-}$ females ($n = 2.8 \pm 1.1$) compared to SAFB1$^{+/+}$ ($n = 5.3 \pm 1.9$) and SAFB1$^{+/-}$ ($n = 5.6 \pm 2.9$) females. Histological analysis revealed no major defects in the oviduct, although a thinner muscle layer in the oviductal wall was noticed in four out of six SAFB1$^{-/-}$ females analyzed (Fig. 5B). Additionally, the oviduct was disproportionally small and showed atrophy that increased with age (Fig. 5C). While this could cause transport defects, other yet to be defined problems might contribute. Collectively, these data suggest that preimplantation development is grossly normal before 3 dpc in SAFB1$^{-/-}$ females and that pregnancies are lost, at least in part, because of defects in oviductal transport.

During regular breeding, we also noted that SAFB1$^{-/-}$ females displayed secondary infertility. To study this in detail, SAFB1$^{-/-}$ female mice ($n = 7$) that had previously given birth were continuously bred for 4 to 5 months, but they did not produce any further litters. This observation, taken together with the findings of fewer embryos at 3.5 dpc (see above) and smaller litter sizes (Table 3), indicated a possible defect in the development and/or maturation of germ cells. GCNA-1 staining of newborn embryos did not reveal any significant changes in the number of germ cells (data not shown), but by 4 weeks of age the number of primordial and primary follicles was significantly decreased (Fig. 5D). There was no difference in the number of secondary follicles between SAFB1$^{+/+}$ and SAFB1$^{-/-}$ mouse ovaries at 4 weeks of age, but there were significantly fewer secondary follicles in older SAFB1$^{-/-}$ mouse ovaries (Fig. 5D). This decrease in follicle number was associated with significant atrophy of the ovaries (Fig. 5E). Thus, the secondary infertility in SAFB1$^{-/-}$ females is likely a result of loss of follicles associated with increasing atrophy of the ovaries and oviducts.

Finally, we asked whether SAFB1 loss would cause altered hormone responses that are intrinsic to SAFB1$^{-/-}$ cells. Therefore, we compared ERE-Tk-Luc reporter assays of SAFB1$^{+/+}$ and SAFB1$^{-/-}$primary MEFs transfected with ERα and subsequently treated with estradiol. As shown in Fig. 5F, estrogen-induced ERα activity was significantly higher in SAFB1$^{-/-}$ cells. Similar results were obtained in a second MEF pair, as well as in immortalized MEF clones (data not shown). Thus, the phenotypes in the reproductive systems of the SAFB1$^{-/-}$ mice reflect changes in systemic hormone levels, as well as cell-intrinsic defects due to the loss of a transcriptional repressor.

DISCUSSION

SAFB1 was originally described as an S/MAR-binding protein, and a number of functions in different cellular processes, such as chromatin organization, RNA processing (29, 36), transcriptional repression (47), and stress response (13), have since been ascribed to it. However, to date there has been no evidence for the physiological role of SAFB1 in vivo. To address this issue, we performed targeted gene mutation of mice and herein demonstrate that SAFB1 is involved in embryonic development, growth control, and regulation of fertility.

Deletion of SAFB1 resulted in death at two time points (before E10.5 and shortly after birth), implying multiple functions of SAFB1 during development, and in particular during embryogenesis. Intriguingly, haploinsufficiency in SAFB1 also reduced survival, whereas many other phenotypes found in SAFB$^{-/-}$ mice were not observed in SAFB1$^{+/-}$ mice. The variable penetrance of the defect resulting in lethality also suggests the presence of genetic modifiers, since these studies were performed with mice with a mixed genetic background (C57BL/6J × 129/Sv).

The finding that circulating IGF1 is reduced in SAFB1$^{-/-}$ mice may explain some of the observed phenotypes. For example, targeted gene deletion of IGF1 has shown that it is critical for both embryonic and postnatal growth (4, 33), so that the reduction in IGF1 in SAFB1$^{-/-}$ mice could account for the in utero growth retardation. Similarly, IGF1 is also important for gonadal function. Several models of dwarf mice (e.g., ames, pigmy, and Snell) (10, 11), as well as both IGF1$^{-/-}$ (4) and growth hormone receptor$^{-/-}$ (8, 9) mice, have small testes, low testosterone levels, and poor sperm production. Supporting this, blockade of IGF1 action by overexpression of IGF-binding protein 1 in mice also causes male infertility due to small testes, low testosterone levels, and poor sperm production

(20). IGF1 acts both on the gonadotropin-releasing hormone axis (22) and directly on the testes to regulate both steroidogenesis and spermatogenesis. In fact, Leydig cells express IGF1R (31), and their proliferation, differentiation, and testosterone production are stimulated by IGF1 in vitro and in vivo (44, 49). The low testosterone levels in SAFB1$^{-/-}$ males might also result from altered expression of steroidogenesis enzymes since IGF1 has been shown to directly affect their expression (32).

We do not fully understand the molecular interaction between SAFB1 and the IGF1 system. More studies are necessary and will yield important, broadly applicable information since defects in the IGF system are common among a number of mouse models with alterations in nuclear hormone receptor cofactors. For example, SRC3$^{-/-}$ mice are born small and have reduced circulating IGF1 levels (50, 53). Importantly, MEFs derived from these mice are also refractory to IGF1-mediated proliferation (50) and migration (26), indicating a cell-intrinsic effect from loss of SRC3. In contrast, we have found that SAFB1$^{-/-}$ MEFs actually showed an increased IGF1 response. This would be consistent with coactivators such as SRC3 increasing the IGF response, while corepressors such as SAFB1 decrease the IGF1 response.

In females, IGF1 is thought to regulate many aspects of ovarian function, particularly during follicular growth (1, 4, 43). The reduction in fertility in SAFB1$^{-/-}$ mice may be due to the observed reduction in follicle numbers, which is similar to what has been described for female mice lacking IRS-2, a component of the IGF-1 signaling cascade (7). Similarly, disruption of another signaling intermediate in the IGF pathway, SH2-B, also results in female mice that are subfertile with fewer follicles (40). While this might contribute to the observed reduction of fertility in the SAFB1$^{-/-}$ mice, there are clearly additional reasons for the impaired fertility. These include defects in development and/or function of the oviducts and increasing atrophy of the ovaries. Importantly, cell-intrinsic defects may also contribute to the observed phenotypes. SAFB1$^{-/-}$ MEFs display an increased response to estrogen, as one would expect from the loss of an ERα corepressor. To our knowledge, this is the first evidence that loss of an ERα corepressor results in an increased estrogen response. MEFs lacking another ERα corepressor, NCoR, showed antiestrogen agonism but no significant change in estrogen-mediated ERα activity (24). Deletion of BRCA1, which was also shown to function as an ERα corepressor (17, 18), resulted in decreased estrogen-mediated ERα activity (54). In any case, these data have to be interpreted with caution since ERα activity is regulated by multimeric complexes containing proteins that often compensate for each other. Further molecular characterizations are necessary to fully understand and interpret these findings.

To a large extent, this study focused on the characterization of the reproductive organs of SAFB1$^{-/-}$ mice. However, future studies might define additional phenotypes. For example, it will be of interest to analyze whether there are phenotypes in T-cell development such as those described for SATB1 null mice. In these mice, deletion of SATB1 resulted in multiple defects at almost every developmental stage of T-cell development that are associated with changes in hundreds of genes as measured by cDNA microarrays. These observations led the authors to conclude that SATB1 is involved in controlling spatial and temporal gene expression. It is possible that SAFB1, via its SAF-Box, plays a similar role in global gene regulation. Ongoing microarray studies in our laboratory will help to define this potential role of SAFB1.

The number and severity of abnormalities in SAFB1$^{-/-}$ mice call into the question the role of its closely related paralogue SAFB2 (46). The two proteins have a very high level of similarity in a number of functional domains, but it appears that SAFB2 is not able to compensate for SAFB1 deficiency. Further studies are necessary to determine which functions are additive, synergistic, compensatory, or even antagonistic between SAFB1 and SAFB2. Toward this goal, we are currently generating mice with a targeted deletion of the gene for SAFB2.

In summary, genetic deletion of SAFB1 results in a number of defects, including prenatal and neonatal lethality, dwarfism, and reduced sexual and reproductive functions. These defects are likely to result from changes in sex hormones and IGF1 levels, as well as altered hormone response resulting from loss of SAFB1-mediated repression of hormone receptors.

ACKNOWLEDGMENTS

This work was supported by NIH grants R01 CA92713 (S.O.) and R01 CA94118 (A.V.L.), NIH program project grant P01 CA030195 (principal investigator, C. K. Osborne; project leader, S.O.), a Chao award (S.O.), a Women in Endocrinology award (S.O.), and postdoctoral (M.I.) (DAMD 17-01-Q1-0136) and predoctoral (K.D.) (W81XWH 04-01-0355) fellowships from the Department of Defense.

We thank F. DeMayo (BCM) at the Transgenic Core for outstanding service and continuing support throughout the project; Earlene Schmitt (BCM) for helping with the ES cell work; G. C. Enders, University of Kansas Medical Center, for providing GCNA antibodies; Ora Britton (BCM) for outstanding technical support; A. I. Agoulnik (BCM) for help with the analysis of the male reproductive system; J. Richards (BCM) for help with the ovary analysis and critical reading of the manuscript; S. Mohsin and staff at the Breast Center Pathology Core (BCM) for outstanding service and helpful discussion; R. Behringer (M. D. Anderson Cancer Center, Houston, Tex.) for providing the pNTRLacZPGKneolox plasmid; M. Matzuk and G. Chamness (BCM) for critical review of the manuscript; and Heidi Weiss (BCM) at the Breast Center Biostatistical Core for the statistical analysis.

REFERENCES

1. **Adashi, E. Y., C. E. Resnick, A. J. D'Ercole, M. E. Svoboda, and J. J. Van Wyk.** 1985. Insulin-like growth factors as intraovarian regulators of granulosa cell growth and function. Endocr. Rev. **6:**400–420.
2. **Alvarez, J. D., D. H. Yasui, H. Niida, T. Joh, D. Y. Loh, and T. Kohwi-Shigematsu.** 2000. The MAR-binding protein SATB1 orchestrates temporal and spatial expression of multiple genes during T-cell development. Genes Dev. **14:**521–535.
3. **Aravind, L., and E. V. Koonin.** 2000. SAP—a putative DNA-binding motif involved in chromosomal organization. Trends Biochem. Sci. **25:**112–114.
4. **Baker, J., J. P. Liu, E. J. Robertson, and A. Efstratiadis.** 1993. Role of insulin-like growth factors in embryonic and postnatal growth. Cell **75:**73–82.
5. **Bode, J., C. Benham, A. Knopp, and C. Mielke.** 2000. Transcriptional augmentation: modulation of gene expression by scaffold/matrix-attached regions (S/MAR elements). Crit. Rev. Eukaryot. Gene Expr. **10:**73–90.
6. **Bonnerot, C., and J. F. Nicolas.** 1993. Application of LacZ gene fusions to postimplantation development. Methods Enzymol. **225:**451–469.
7. **Burks, D. J., J. F. de Mora, M. Schubert, D. J. Withers, M. G. Myers, H. H. Towery, S. L. Altamuro, C. L. Flint, and M. F. White.** 2000. IRS-2 pathways integrate female reproduction and energy homeostasis. Nature **407:**377–382.
8. **Chandrashekar, V., A. Bartke, C. A. Awoniyi, C. H. Tsai-Morris, M. L. Dufau, L. D. Russell, and J. J. Kopchick.** 2001. Testicular endocrine function in GH receptor gene disrupted mice. Endocrinology **142:**3443–3450.
9. **Chandrashekar, V., A. Bartke, K. T. Coschigano, and J. J. Kopchick.** 1999. Pituitary and testicular function in growth hormone receptor gene knockout mice. Endocrinology **140:**1082–1088.
10. **Chubb, C.** 1989. Genetically defined mouse models of male infertility. J. Androl. **10:**77–88.

11. **Chubb, C., and C. Nolan.** 1985. Animal models of male infertility: mice bearing single-gene mutations that induce infertility. Endocrinology **117:** 338–346.
12. **Couse, J. E., D. Mahato, E. M. Eddy, and K. S. Korach.** 2001. Molecular mechanism of estrogen action in the male: insights from the estrogen receptor null mice. Reprod. Fertil. Dev. **13:**211–219.
13. **Denegri, M., I. Chiodi, M. Corioni, F. Cobianchi, S. Riva, and G. Biamonti.** 2001. Stress-induced nuclear bodies are sites of accumulation of pre-mRNA processing factors. Mol. Biol. Cell **12:**3502–3514.
14. **Dobrzycka, K. M., S. M. Townson, S. Jiang, and S. Oesterreich.** 2003. Estrogen receptor corepressors—a role in human breast cancer? Endocr. Relat. Cancer **10:**517–536.
15. **Emmen, J. M., and K. S. Korach.** 2003. Estrogen receptor knockout mice: phenotypes in the female reproductive tract. Gynecol. Endocrinol. **17:**169–176.
16. **Enders, G. C., and J. J. May II.** 1994. Developmentally regulated expression of a mouse germ cell nuclear antigen examined from embryonic day 11 to adult in male and female mice. Dev. Biol. **163:**331–340.
17. **Fan, S., Y. X. Ma, C. Wang, R. Q. Yuan, Q. Meng, J. A. Wang, M. Erdos, I. D. Goldberg, P. Webb, P. J. Kushner, R. G. Pestell, and E. M. Rosen.** 2001. Role of direct interaction in BRCA1 inhibition of estrogen receptor activity. Oncogene **20:**77–87.
18. **Fan, S., J.-A. Wang, R. Yuan, Y. Ma, Q. Meng, M. R. Erdos, R. G. Pestell, F. Yuan, K. J. Auborn, I. D. Goldberg, and E. M. Rosen.** 1999. BRCA1 inhibition of estrogen receptor signaling in transfected cells. Science **284:** 1354–1356.
19. **Frasor, J., F. Stossi, J. M. Danes, B. Komm, C. R. Lyttle, and B. S. Katzenellenbogen.** 2004. Selective estrogen receptor modulators: discrimination of agonistic versus antagonistic activities by gene expression profiling in breast cancer cells. Cancer Res. **64:**1522–1533.
20. **Froment, P., C. Staub, S. Hembert, C. Pisselet, M. Magistrini, B. Delaleu, D. Seurin, J. E. Levine, L. Johnson, M. Binoux, and P. Monget.** 2004. Reproductive abnormalities in human insulin-like growth factor-binding protein-1 transgenic male mice. Endocrinology **145:**2080–2091.
21. **Gehin, M., M. Mark, C. Dennefeld, A. Dierich, H. Gronemeyer, and P. Chambon.** 2002. The function of TIF2/GRIP1 in mouse reproduction is distinct from those of SRC-1 and p/CIP. Mol. Cell. Biol. **22:**5923–5937.
22. **Hiney, J. K., V. Srivastava, C. L. Nyberg, S. R. Ojeda, and W. L. Dees.** 1996. Insulin-like growth factor I of peripheral origin acts centrally to accelerate the initiation of female puberty. Endocrinology **137:**3717–3728.
23. **Honda, J., Y. Manabe, R. Matsumura, S. Takeuchi, and S. Takahashi.** 2003. IGF-I regulates pro-opiomelanocortin and GH gene expression in the mouse pituitary gland. J. Endocrinol. **178:**71–82.
24. **Jepsen, K., O. Hermanson, T. M. Onami, A. S. Gleiberman, V. Lunyak, R. J. McEvilly, R. Kurokawa, V. Kumar, F. Liu, E. Seto, S. M. Hedrick, G. Mandel, C. K. Glass, D. W. Rose, and M. G. Rosenfeld.** 2000. Combinatorial roles of the nuclear receptor corepressor in transcription and development. Cell **102:**753–763.
25. **Kipp, M., F. Göhring, T. Ostendorp, C. M. van Drunen, R. van Driel, M. Przybylski, and F. O. Fackelmayer.** 2000. SAF-Box, a conserved protein domain that specifically recognizes scaffold attachment region DNA. Mol. Cell. Biol. **20:**7480–7489.
26. **Kuang, S. Q., L. Liao, H. Zhang, A. V. Lee, B. W. O'Malley, and J. Xu.** 2004. AIB1/SRC-3 deficiency affects insulin-like growth factor I signaling pathway and suppresses v-Ha-ras-induced breast cancer initiation and progression in mice. Cancer Res. **64:**1875–1885.
27. **Lee, A. V., S. T. Taylor, J. Greenall, J. D. Mills, D. W. Tonge, P. Zhang, J. George, M. L. Fiorotto, and D. L. Hadsell.** 2003. Rapid induction of IGF-IR signaling in normal and tumor tissue following intravenous injection of IGF-I in mice. Horm. Metab. Res. **35:**651–655.
28. **Leonardsson, G., M. A. Jacobs, R. White, R. Jeffery, R. Poulsom, S. Milligan, and M. Parker.** 2002. Embryo transfer experiments and ovarian transplantation identify the ovary as the only site in which nuclear receptor interacting protein 1/RIP140 action is crucial for female fertility. Endocrinology **143:** 700–707.
29. **Li, J., I. C. Hawkins, C. D. Harvey, J. L. Jennings, A. J. Link, and J. G. Patton.** 2003. Regulation of alternative splicing by SRrp86 and its interacting proteins. Mol. Cell. Biol. **23:**7437–7447.
30. **Liao, L., S. Q. Kuang, Y. Yuan, S. M. Gonzalez, B. W. O'Malley, and J. Xu.** 2002. Molecular structure and biological function of the cancer-amplified nuclear receptor coactivator SRC-3/AIB1. J. Steroid Biochem. Mol. Biol. **83:**3–14.
31. **Lin, T., J. Blaisdell, and J. F. Haskell.** 1988. Hormonal regulation of type I insulin-like growth factor receptors of Leydig cells in hypophysectomized rats. Endocrinology **123:**134–139.
32. **Lin, T., J. Haskell, N. Vinson, and L. Terracio.** 1986. Characterization of insulin and insulin-like growth factor I receptors of purified Leydig cells and their role in steroidogenesis in primary culture: a comparative study. Endocrinology **119:**1641–1647.
33. **Liu, J. P., J. Baker, A. S. Perkins, E. J. Robertson, and A. Efstratiadis.** 1993. Mice carrying null mutations of the genes encoding insulin-like growth factor I (Igf-1) and type 1 IGF receptor (IGF1r). Cell **75:**59–72.
34. **Livak, K. J., and T. D. Schmittgen.** 2001. Analysis of relative gene expression data using real-time quantitative PCR and the $2^{-\Delta\Delta}$Cr method. Methods **25:**402–408.
35. **McLeod, M. J.** 1980. Differential staining of cartilage and bone in whole mouse fetuses by alcian blue and alizarin red S. Teratology **22:**299–301.
36. **Nayler, O., W. Stratling, J. P. Bourquin, I. Stagljar, L. Lindemann, H. Jasper, A. M. Hartmann, F. O. Fackelmayer, A. Ullrich, and S. Stamm.** 1998. SAF-B protein couples transcription and pre-mRNA splicing to SAR/MAR elements. Nucleic Acids Res. **26:**3542–3549.
37. **Oesterreich, S.** 2003. Scaffold attachment factors SAFB1 and SAFB2: innocent bystanders or critical players in breast tumorigenesis? J. Cell. Biochem. **90:**653–661.
38. **Oesterreich, S., A. V. Lee, T. M. Sullivan, S. K. Samuel, J. R. Davie, and S. A. Fuqua.** 1997. Novel nuclear matrix protein HET binds to and influences activity of the HSP27 promoter in human breast cancer cells. J. Cell. Biochem. **67:**275–286.
39. **Oesterreich, S., Q. Zhang, T. Hopp, S. A. Fuqua, M. Michaelis, H. H. Zhao, J. R. Davie, C. K. Osborne, and A. V. Lee.** 2000. Tamoxifen-bound estrogen receptor (ER) strongly interacts with the nuclear matrix protein HET/SAF-B, a novel inhibitor of ER-mediated transactivation. Mol. Endocrinol. **14:**369–381.
40. **Ohtsuka, S., S. Takaki, M. Iseki, K. Miyoshi, N. Nakagata, Y. Kataoka, N. Yoshida, K. Takatsu, and A. Yoshimura.** 2002. SH2-B is required for both male and female reproduction. Mol. Cell. Biol. **22:**3066–3077.
41. **Ratts, V. S., J. A. Flaws, R. Kolp, C. M. Sorenson, and J. L. Tilly.** 1995. Ablation of bcl-2 gene expression decreases the numbers of oocytes and primordial follicles established in the post-natal female mouse gonad. Endocrinology **136:**3665–3668.
42. **Renz, A., and F. O. Fackelmayer.** 1996. Purification and molecular cloning of the scaffold attachment factor B (SAF-B), a novel human nuclear protein that specifically binds to S/MAR-DNA. Nucleic Acids Res. **24:**843–849.
43. **Richards, J. S., D. L. Russell, S. Ochsner, M. Hsieh, K. H. Doyle, A. E. Falender, Y. K. Lo, and S. C. Sharma.** 2002. Novel signaling pathways that control ovarian follicular development, ovulation, and luteinization. Recent Prog. Horm. Res. **57:**195–220.
44. **Rouiller-Fabre, V., L. Lecref, C. Gautier, J. M. Saez, and R. Habert.** 1998. Expression and effect of insulin-like growth factor I on rat fetal Leydig cell function and differentiation. Endocrinology **139:**2926–2934.
45. **Tilly, J. L.** 2003. Ovarian follicle counts—not as simple as 1, 2, 3. Reprod. Biol. Endocrinol. **1:**11.
46. **Townson, S. M., K. M. Dobrzycka, A. V. Lee, M. Air, W. Deng, K. Kang, S. Jiang, N. Kioka, K. Michaelis, and S. Oesterreich.** 2003. SAFB2, a new scaffold attachment factor homolog and estrogen receptor corepressor. J. Biol. Chem. **278:**20059–20068.
47. **Townson, S. M., K. Kang, A. V. Lee, and S. Oesterreich.** 2004. Structure-function analysis of the estrogen receptor alpha corepressor scaffold attachment factor-B1: identification of a potent transcriptional repression domain. J. Biol. Chem. **279:**26074–26081.
48. **Vecchi, A., C. Garlanda, M. G. Lampugnani, M. Resnati, C. Matteucci, A. Stoppacciaro, H. Schnurch, W. Risau, L. Ruco, A. Mantovani, et al.** 1994. Monoclonal antibodies specific for endothelial cells of mouse blood vessels. Their application in the identification of adult and embryonic endothelium. Eur. J. Cell Biol. **63:**247–254.
49. **Wang, G., and M. P. Hardy.** 2004. Development of Leydig cells in the insulin-like growth factor-I (igf-I) knockout mouse: effects of igf-I replacement and gonadotropic stimulation. Biol. Reprod. **70:**632–639.
50. **Wang, Z., D. W. Rose, O. Hermanson, F. Liu, T. Herman, W. Wu, D. Szeto, A. Gleiberman, A. Krones, K. Pratt, R. Rosenfeld, C. K. Glass, and M. G. Rosenfeld.** 2000. Regulation of somatic growth by the p160 coactivator p/CIP. Proc. Natl. Acad. Sci. USA **97:**13549–13554.
51. **Weighardt, F., F. Cobianchi, L. Cartegni, I. Chiodi, A. Villa, S. Riva, and G. Biamonti.** 1999. A novel hnRNP protein (HAP/SAF-B) enters a subset of hnRNP complexes and relocates in nuclear granules in response to heat shock. J. Cell Sci. **112:**1465–1476.
52. **White, R., G. Leonardsson, I. Rosewell, M. Ann Jacobs, S. Milligan, and M. Parker.** 2000. The nuclear receptor co-repressor nrip1 (RIP140) is essential for female fertility. Nat. Med. **6:**1368–1374.
53. **Xu, J., L. Liao, G. Ning, H. Yoshida-Komiya, C. Deng, and B. W. O'Malley.** 2000. The steroid receptor coactivator SRC-3 (p/CIP/RAC3/AIB1/ACTR/TRAM-1) is required for normal growth, puberty, female reproductive function, and mammary gland development. Proc. Natl. Acad. Sci. USA **97:**6379–6384.
54. **Zheng, L., L. A. Annab, C. A. Afshari, W. H. Lee, and T. G. Boyer.** 2001. BRCA1 mediates ligand-independent transcriptional repression of the estrogen receptor. Proc. Natl. Acad. Sci. USA **98:**9587–9592.